Effects of Soil Characteristics on Evapotranspiration-Driven Water Table Decline and Recovery in a Forested Floodplain

Samantha Volz

Advisors: Dr. Karen Prestegaard
Graduate Student: Haley Talbot-Wendlandt
GEOL 394

Abstract

The objective of this study is to examine relationships among vegetation, hydrology, soil characteristics and their influences on water table depth in a temperate forest. Evapotranspiration (ET) and precipitation (PPT) are the largest terms in the water balance, however, water table responses are also affected by soil properties and vegetation, including parameters such as soil bulk density, organic matter content, capillary fringe height, and soil texture. A simple water balance equation is used to explain the change in groundwater storage: Δ storage = PPT – ET. In this study, vegetation and soil characteristics were measured at two sites (floodplain and terrace) in a forest. Precipitation was monitored, along with other meteorological data that were used to calculate evapotranspiration. Groundwater wells were monitored for one year at both the floodplain and terrace sites. Soil infiltration capacity was measured at the field sites. Soil cores at two sites were used to determine soil characteristic (bulk density, organic matter content, porosity, and grain size). Three hypotheses were tested: a) groundwater minima are driven by evapotranspiration in excess of precipitation; b) Soil characteristics (bulk density, organic matter) are influenced near the surface by biota (roots and organisms), which results in a vertical change in soil properties with depth; c) the capillary fringe height primarily reflects effective matrix pore size and will remain constant as the groundwater table declines. Organic matter decreases with depth, bulk density increased with depth, and porosity decreased with depth at both the floodplain and lower floodplain sites. These key characteristics are used to evaluate macroporosity, predict capillary fringe responses, and compare with measured infiltration rates. Groundwater well data indicates groundwater declines throughout the summer months with fall minima and recovering during the fall/winter months.

Introduction

The effects of vegetation, soil properties, evapotranspiration (ET), and precipitation (PPT) are all interconnected, and they are important factors that influence groundwater table fluctuations (Fig. 1). In a homogeneous soil, a simple bucket model can be used to evaluate a simple water balance: PPT- ET = D Groundwater Storage (Zhang et al. 2002). Soil characteristics and rooting density, however, also affect water table responses. The rate and magnitude of water table responses can be influenced by macropore density, capillary fringe height, rooting depth and density, and soil permeability (infiltration rate and hydraulic conductivity). The objective of this research is to examine the relationships among ET demand, soil type and hydraulic properties to see how they explain water table responses in a forested floodplain. This work will evaluate how groundwater storage responds to recharge during storms and withdrawal due to ET over an annual cycle in a climatic region where ET is the water balance component that varies the most.

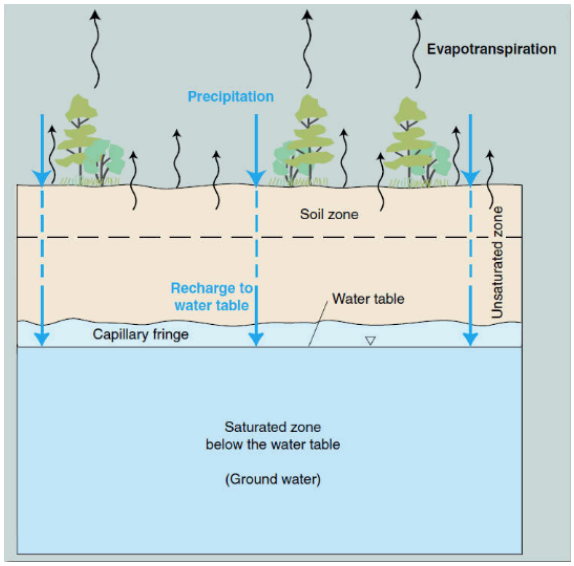

Fig. 1: Basic representation of the water table, saturated zone, unsaturated zone, and basic water balance. (USGS)

Soil properties can directly affect the groundwater response to storm events and ET, and thus groundwater storage. An simplified model of groundwater storage for a flat floodplain is: D storage = PPT – ET, but this simple model assumes that soil properties are homogeneous, and that groundwater drainage is constant or absent. Groundwater level changes as water volume is added to or removed from the soil. The change in groundwater level = water added or removed (mm) multiplied by the specific yield of the soil. The specific yield = porosity -specific retention, and this is usually a function of grain size and other soil characteristics. By obtaining soil cores at two locations near the sites where groundwater is monitored, porosity can be estimated from the bulk density and organic matter content of the soil; these parameters in addition to grain size can be used to determine specific yield and to examine how both porosity and specific yield vary in each layer in a soil profile.

Background

Soil plays an important role in regulating Earth's climate. Soil stores more organic carbon than the atmosphere and global vegetation combined (Lehmann and Kleber, 2015). Leaf litter and tree roots are large contributors to soil organic matter, but soil organic matter storage is sensitive to climate and soil wetness. Fan et al. (2017) presented a general relationship between plant rooting depth and water table depth. Water table can vary regionally, and can reflect variations in climate, vegetation, and topography. Tree roots can form at different depths in soils or even be bimodally distributed so that they can intercept infiltrating water and/or obtain water from depth during periods of water table minimum. If trees obtain most of their water by intercepting infiltrating water, then rooting depths should be shallow and distributed laterally. Tree water demand would also set the spacing of trees and perhaps their maximum growth height. If trees obtain water primarily from deeper groundwater

horizons and the capillary fringe, roots will tend to be deeper, leading to vertical roots into the capillary fringe (Fan et al. 2017). A tree could have dimorphic roots to obtain water from both sources (Fig. 2). Though tree genera are adapted to location, wetland-tolerant genera tend to have shallower roots and arid-tolerant species tend to have deeper roots as an adaptation to warm-dry climates or seasonally distributed rainfall. Some tree species have wide ranges of possible rooting depths, suggesting that they can adapt to local environments. However, soil properties and bedrock depth also influence rooting depths and styles. Trees can be resilient to environmental stress and adapt to inter-annual differences in hydrological conditions, but it is unknown how they will adapt to the rapidly changing global climate (Fan et al. 2017).

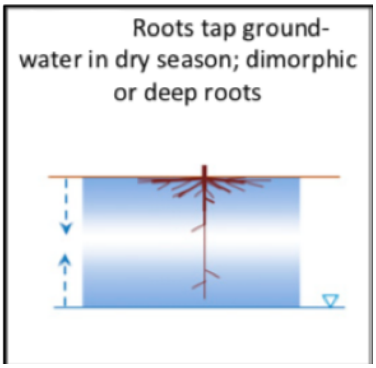

Fig. 2: Trees can have both shallow and deep roots to access changing water availability. (Fan et al. 2017)

The relationships among soil characteristics, hydrology, and groundwater response are complex, but this research is focused on the interactions between soil properties and hydrological parameters in a site selected in part for its homogeneous forest cover. Infiltration capacity is the rate at which water can be moved downward into the soil, which is regulated by the downward movement of wetting fronts (Nimmo et al. 2009). The maximum infiltration rate can be significantly higher than matrix infiltration rates, because it also includes macropore infiltration. Matrix infiltration is the capillary pull of water into dry soils, filling of pore spaces, and macropore flows the movement of water into larger pore spaces, which are gravitationally drained (Beven and Germann, 1982; Zhang et al. 2017). Saturated hydraulic conductivity (K), an important parameter influencing of infiltration and groundwater flow, at the soil surface it will be determined from data collected using a falling head, single-ring infiltrometer in the field. Other factors that influence infiltration are soil type (grain size and texture), vegetation coverage, and soil moisture.

A simple water balance equation describes general groundwater fluctuation pattern, but the hydrological system is much more complex. The details in groundwater decline and recovery will be affected by roots and soil characteristics. For example, macropores would increase the rate of infiltration, and root density will affect the amount of PPT that would reach the water table. The goal of this research is to provide a better understanding of a seemingly simple system with many complex factors.

Hypotheses

The hypotheses to be tested are:

- In Maryland, groundwater minima are driven by evapotranspiration in excess of precipitation, which removes groundwater storage creating groundwater minima in early autumn.
- Soil characteristics (bulk density, organic matter) are influenced near the surface by biota (roots and organisms), which results in a vertical change in soil properties with depth.
- The capillary fringe height primarily reflects effective matrix pore size, which can be estimated by grain size, and will remain constant as the groundwater table declines.

Soil Hydraulic Properties

Many of the field and laboratory methods that I use in this study are designed to evaluate soil hydraulic properties including: hydraulic conductivity, porosity, bulk density, and grain size. In this section, I define these properties and present methods used to obtain them.

Hydraulic Conductivity

Infiltration-based methods to determine K have been described by Nimmo et al. (2009). Their expression for the field-saturated hydraulic conductivity (K_{fs}) is:

$$K_{fs} = \frac{L_g}{t_f} \ln\left(1 + \frac{D_0}{L_G + \lambda}\right) \qquad (1)$$

where D_o is the initial head, L_G is the installation scale length, defined as: $L_G = C_1 d + C_2 b$ (d is installed depth, b is infiltrometer radius; and all dimensioned values are in cm; C_1 and C_2 are empirically determined constants where $C_1 = 0.993$, $C_2 = 0.578$); and t_f = infiltration time. The value of λ is an index of the effect of capillary forces is on lateral movement. For most soils the values of λ is about 0.08 m, but for fine-textured soil without macropores the value may up to 0.25 m or for gravel with little effective capillary action the value may go as low as 0.03 m (Nimmo et al. 2009).

Capillary Fringe Height

Soil saturation levels is also affected by the extent of the capillary fringe, a zone directly above the water table, where groundwater is drawn up by the capillary action into the pores in the sediment. The height of the capillary fringe above the water table is inversely related to pore size, thus the capillary fringe height would be larger in finer-textured soils and smaller in coarse-textured soils (Cloke et al. 2006). The effective pore radius in the capillary response can be calculated from a manipulation of the standard equations for capillary fringe from Bear (1972):

$$R = \frac{2\gamma cos\Theta}{\rho g h_c} \qquad (2)$$

where R is pore radius; γ is the surface tension of water which is 72.9 N/m; θ is the wetting angle which is ~1 for mineral soils; ρ is water density which is 1000 kg/m^3; g is gravity which is 9.814 m/s^2; h_c is the capillary rise height (Bear 1972). The capillary fringe response rate can be measured using groundwater series data and used to calculate effective pore radius.

Calculation of Evapotranspiration from Climatic Data

Climate directly effects PPT and ET, which are primary components in the local water balance and the major controls on groundwater levels. ET is the combination of ground surface evaporation and plant transpiration. In a flat forested floodplain without local incoming groundwater, the change in water table depth (ΔS) is influenced by the local water balance: ΔS = PPT – ET. Seasonal fluxes in water table depths and ET are connected to temperature and precipitation patterns (Gribovszki et al. 2008). The

Hargreaves-Samani Equation from Ravazzani et al. (2012) is used to calculate daily ET with data from local temperature measurements, precipitation, and solar radiation. Long-term climate data will be obtained from the spatially integrated NOAA data available in PRISM Climate Group. Calculated values of PPT – ET will be compared with groundwater data to obtain ΔS (ΔGroundwater level * Specific yield). The Hargreaves-Samani (HS) Equation for calculating daily reference evapotranspiration (ET_0):

$$ET_{0,HS} = HC * R_a * (T_{max} - T_{min})^{HE} \left(\frac{T_{max}+T_{min}}{2} + 17.8\right) \qquad (3)$$

where $ET_{0,HS}$ is the reference evapotranspiration by the HS equation (mm/day); HC is an empirical coefficient (HC=0.0023); R_a is the extraterrestrial radiation (mm/day); HE is an empirical exponent (HE=0.5); T_{max} is the daily maximum air temperature (°C); and T_{min} is the daily minimum air temperature (°C) (Revazzani et al. 2012). The extraterrestrial radiation values are sited in a table from Hargreaves (1994).

Soil Porosity

Porosity is the measure of the amount of void space in a material, which can be filled with air or water. The void spaces and macropores can be created by vegetation root growth or biota residing in the soil. Porosity and specific yield are interconnected, both are calculated from grain size analysis and bulk density. Porosity (n) is defined by:

$$n = \frac{volume\ of\ void\ space}{total\ volume\ of\ soil} = 1 - \frac{bulk\ density}{particle\ density} \qquad (4)$$

Specific yield is the amount of water that will drain under gravity from an aquifer. Specific retention is the volume of water that remains from capillary force and tension after the aquifer is drained (Heath, 1983). The relationship connecting porosity (n), specific yield (S_y), and specific retention (S_r) is:

$$n = S_y + S_n \qquad (5)$$

$$S_y = \frac{V_d}{V_t} \qquad (6)$$

$$S_r = \frac{V_r}{V_t} \qquad (7)$$

where V_t is total volume of the soil sample, V_d is the water drained from the total volume, and V_r is the volume of the water retained in the total volume. Porosity, specific yield, and specific retention are all dimensionless and expressed in percentages (Heath, 1983). The specific yield is estimated based on grain size.

In soil systems, vegetation can affect soil physical properties, which in turn can affect hydrological responses, such as infiltration rates, evapotranspiration rates, and capillary fringe responses. I constructed the diagram below to summarize some of these important interactions among vegetation, soils, and hydrology (Fig. 3).

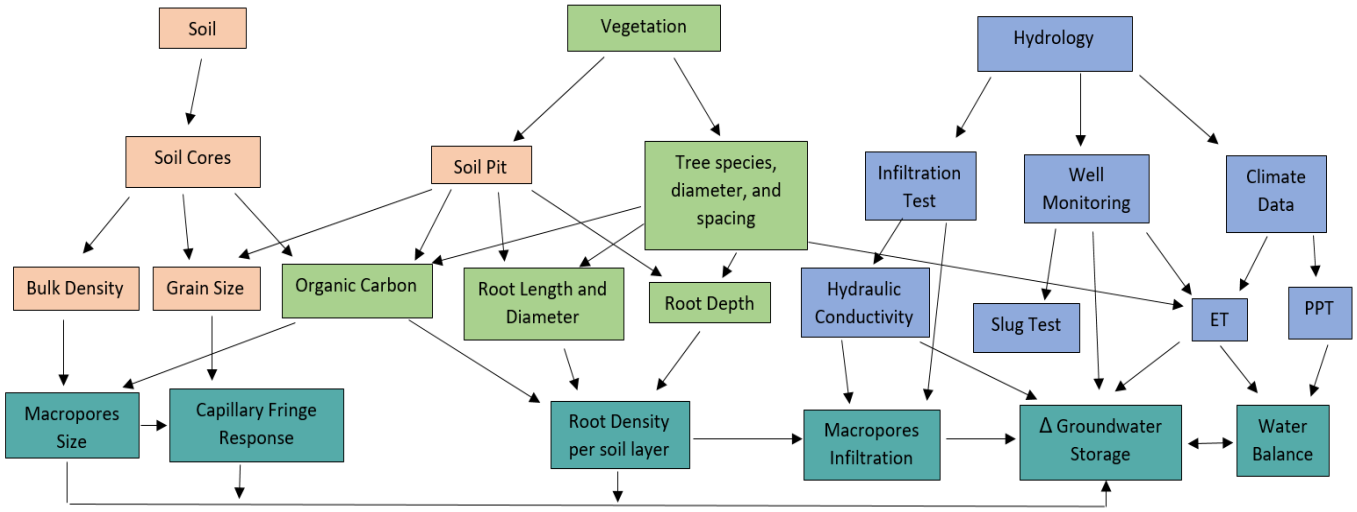

Fig. 3: A ecohydrological interaction flow chart displays the complex interconnection between soil, vegetation, and hydrology aspects and their relations to groundwater storage.

Study Site and Methods

Site Description

The study site is located along the Little Paint Branch (LPB) floodplain in College Park, Maryland (Fig. 4). Dr. Karen Prestegaard and graduate student Haley Talbot-Wendlandt selected three sites to represent the LPB floodplain and installed two groundwater wells at each site in April 2019. The sites were selected to minimize outside influences on the groundwater level by avoiding sites directly next to roads, parking lots, and buildings. The terrace site elevation is 24.4 meters above sea level, and the 2 floodplain sites (named floodplain and hole) are 20.6 meters above sea level. The elevation data was obtained by using State of Maryland LiDAR data and GPS coordinates (Talbot-Wendlandt, personal communication).

Fig. 4: Google Earth image of the 3 study sites on the LPB floodplain in College Park, MD. (Google Earth)

Acquisition of Precipitation and Temperature Data

Precipitation and temperature data are used in water balance calculations and used to calculate ET. A sensor placed at the terrace site recorded temperature and barometric pressure data every 5 minutes. Also, maximum-minimum temperature data and daily precipitation data was obtained from PRISM Climate Group. Monthly 30-year average data are shown below to illustrate seasonal variations in precipitation and temperature (Fig. 5). Atlantic Coast watersheds receive precipitation year-round, but temperature varies seasonally producing seasonal warm months. These variations in temperature and length of day drives seasonal variations in ET.

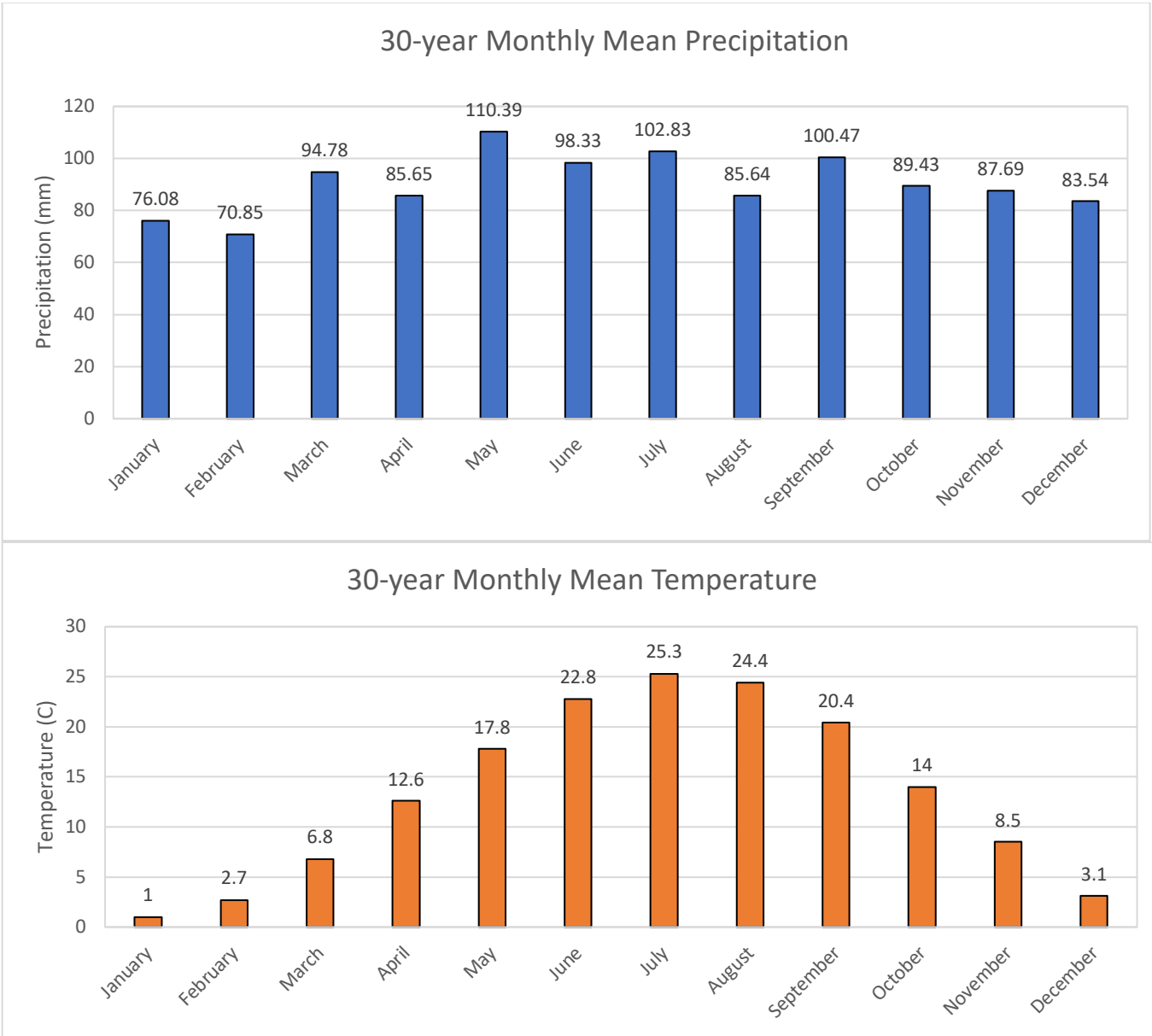

Fig. 5: PRISM Climate Group 30-year average monthly precipitation (top) and temperature (bottom) data for Little Paint Branch (LPB) floodplain between the period 1981 -2010. (PRISM Climate Group)

Groundwater Monitoring

Fig. 6: A groundwater well at the floodplain site.

Each site has one piezometer and one monitoring well, which are constructed of 1.5-meter-long PVC pipe with a HOBO U20 water level logger inserted in each well (Fig. 6). The water level logger data is downloaded approximately once every 1-2 months, and it provides water pressure and temperature data in 5-minute intervals at each site. An additional logger was placed in a tree at the terrace site to record atmospheric pressure and temperature. The monitoring wells allows penetration of water through slits along the length of the PVC pipe below the surface. Conversely, the piezometers only allow water to penetrate at the bottom of the pipe and they measure the pressure only at the bottom pipe. The monitoring wells allow for an overall understanding of the groundwater movement through each site, but the piezometer measures the hydraulic head in the soil.

Tree Identification and Measurements of Tree Size and Density

A 10 x 10 m plot was measured centered around the piezometer at each site. The tree species were identified at each plot and the circumference of each trunk was measured at chest height and recorded. Trees shorter than 1.63 m (my height) were not included in the sample.

Soil Sampling using Soil Pits and Soil Cores

Soil samples were obtained from soil pits and soil cores. Soil pits were used to measure the root density with depth and obtain soil samples at each horizon for later lab analysis, such as grain size, soil bulk density, soil color, and organic content. Soil cores were collected in increments using a hand auger at the floodplain and terrace site. Before collecting the sample, the leaf litter was cleared away from the ground surface. The hand auger was inserted perpendicular to the ground and rotated to cut into the soil. The soil samples were removed in roughly 10 cm increments and carefully placed in plastic bag to not lose any soil. The exact depth of the hole was measured between samples to record the correct increment.

Bulk Density

Bulk density (r) is the mass of the dried soil per total soil volume:

$$\rho = \frac{mass}{volume} \left(\frac{g}{cm^3}\right) \qquad (8)$$

The volume was determined from the diameter of the hand auger (cylinder) and the depth of the increments the soil was extracted. The soil samples were first weighted to obtain the field bulk density, which includes the moisture content of the soil. The samples were then placed in a low temperature oven on a labeled oven safe dish and baked at overnight at 100 °C until completely dry. The dry samples were weighed twice to ensure they were completely dry and to obtain the mass of the dry soil (Al Shammary et al. 2018). Bulk density measurements were used to calculate soil porosity as described earlier.

Soil Organic Matter

After the soil samples are dried for the bulk density determinations, the proportion of organic matter was calculated by the combusting the sediment in the soil samples. First, the dried soil samples were homogenized using a mortar and pestle. After weighing porcelain crucibles, 3 homogenized subsamples from each soil sample collected were measured in the crucibles and placed in a kiln heated to 750 °C for 6 hours. Carbon dioxide is created from the organic matter ignition and combustion. After the time is completed, turn off the kiln and allow samples to cool down for 2 hours before opening the door. After combustion, weight the cooled samples again to determine the mass lost to organic matter.

Grain Size Analysis – Sieve Analysis

Soil texture influences the movement of water, nutrients, and air through soil. Grain size analysis is a test performed to obtain the percentage of different sized grains in a soil sample. First, the dried soil sample total weight is recorded, then break up the soil aggregates using a mortar and pestle. The homogenized sample is carefully poured into the top of a clean stack of descending sized sieves with a pan on the bottom. A cap is place on top sieve and moved to a mechanical shaker, where it shakes for 15 minutes to separate the different grain sizes (Fig. 7). The sieve is removed from the shaker and sediment is carefully weighed in each sieve and the pan at the bottom. The error is calculated by subtracting the original soil sample weight from the sum of the soil weight from each sieve and dividing it by the original sample weight again.

Fig. 7: The mechanical shaker with the stacked sieves.

Falling Head, Single-Ring Infiltrometer

Fig. 8: (Top) A 15.5 cm single-ring infiltrometer during an infiltration test. (Bottom) Measuring the wetting depth, and numerous roots just under the ground surface.

Field-saturated hydraulic conductivity is determined by measuring the rate at which water infiltrates into the soil using a falling head, single-ring infiltrometer. An infiltration ring was made of a can (9.5 or 15.5 cm diameter) with both ends removed with a can opener (Fig. 8). The test area was selected with no vegetation and the leaf litter was removed from the surface. The ring was then gently tapped into the ground using a hammer until the bottom rim could not go any further into the ground, and then gently rocked back and forth to insure a tight seal. The ring must be moved to a new location if the soil around the ring is loose and a tight seal is not formed. A rule was placed into the ring, and water quickly poured directly into the ring to a predetermined height. The rate at which the water infiltrates into the soil is recorded at preset time intervals. Before removing the infiltration ring, the height of the ring was measured above the soil to determine the rings installed depth. After the infiltration test, the area underneath the ring was excavated to measure the wetting depth (Nimmo et al. 2009).

Results and Discussion

Tree Sizing and Spacing

Vegetation is an important factor in understanding the soil characteristic and hydrology in a forested floodplain. The type of tree and root density influences the organic matter, bulk density, ET rates, and groundwater balance. Table 1 contains the tree identification and spacing for each field site. This data was collected with Haley Talbot-Wendlandt.

Site	Total Number of Trees	Dominant Species	Total Tree Area (m^2)	Average Diameter (cm)	Tree Density $\left(m^2/_{m^2}\right)$
Hole	15	Red Maple	0.860	14.82	0.00860
Floodplain	32	White Ash, Shadbush	0.425	10.17	0.00425
Terrace	9	Red Maple	0.517	20.46	0.00517

Table 1: A table containing the total number of trees, dominant species, total tree area, average diameter, and tree density for each site in the LPB system.

Soil Characteristics:

The soil properties include bulk density, porosity, soil organic carbon content, and grain size measured at intervals from soil core samples that were collected above the water table. The data are shown on the following graphs and tables comparing the terrace and floodplain sites during fall and spring.

Bulk Density

The results of the bulk density soil profiles with depth interval for the terrace and floodplain sites are shown in Fig. 9. For reference, a mineral soil without macropores has bulk density of about 1.65 g/cm^3 (Dunne and Leopold, 1978). Bulk density for both sites near the surfaces is low between 0.5-0.8 g/cm^3. The bulk density increases with depth, becoming closer to a mineral soil's averages bulk density. Bulk density typically increases with depth because of less organic matter and root penetration.

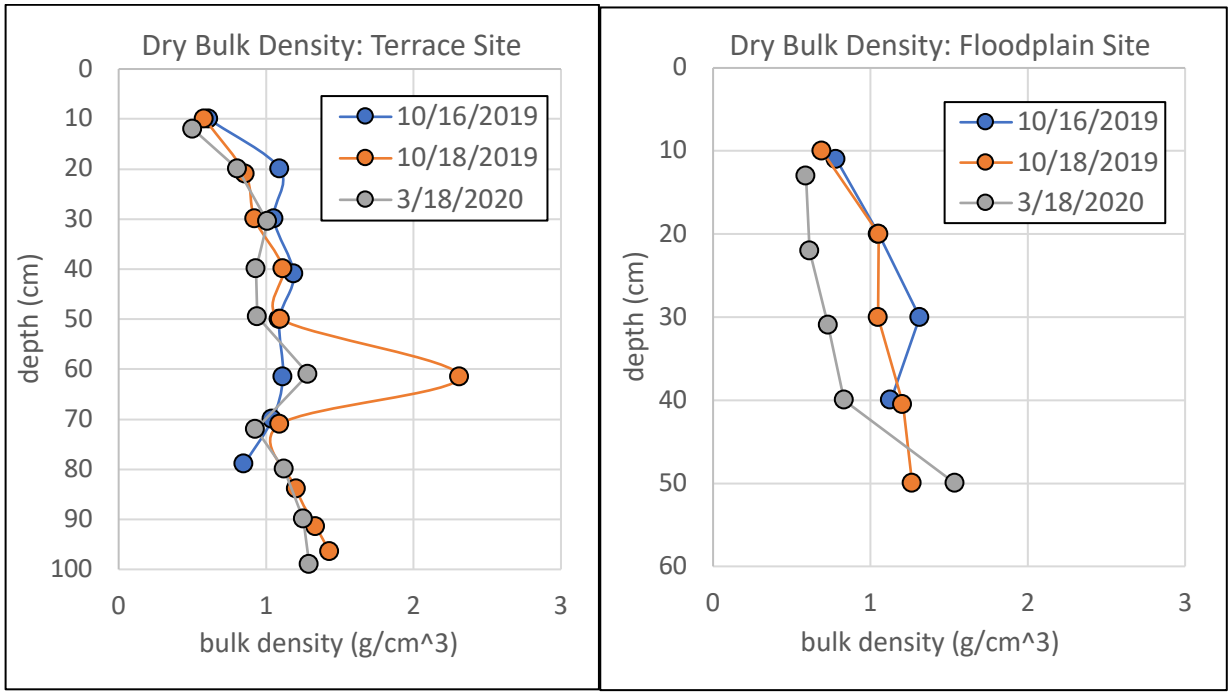

Fig. 9: Dry bulk density at depth intervals for the terrace (left) and floodplain site (right).

Porosity

Porosity is calculated using the bulk density data for each depth interval. The soils density value used is 2.65 g/cm^3 because quartz is the dominant mineral in most soils. For reference, fine grains tend to have higher porosity than coarser grains. Fig. 10 shows the porosity decreases with depth at each site.

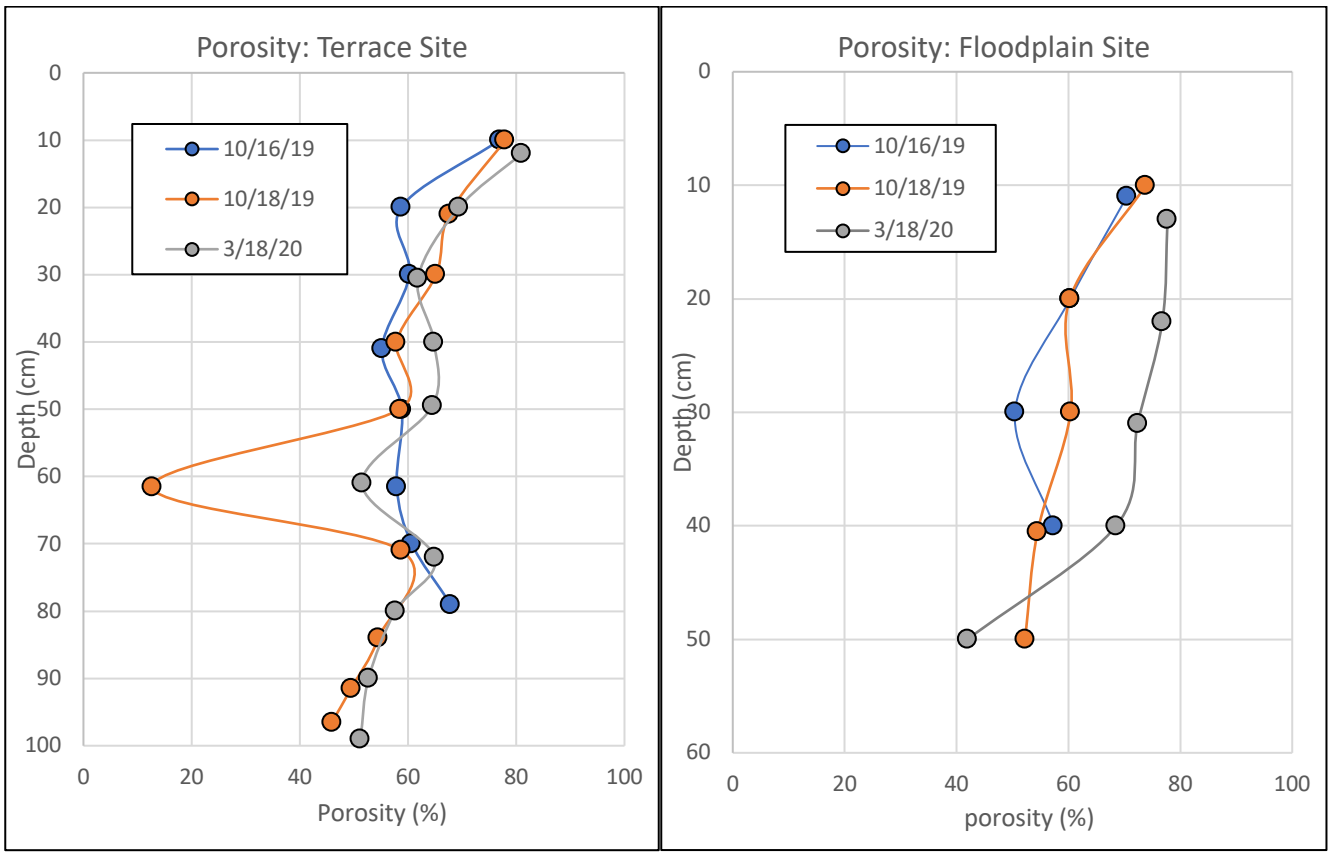

Fig. 10: Porosity calculated using the dry bulk density with depth for the terrace (left) and floodplain site (right).

Soil Organic Carbon

Soil organic carbon was measured by loss on ignition in subsamples of the cores used in the bulk density analyses. Analyses were conducted on 6 total core samples taken at the floodplain and terrace site. The organic carbon is highest near the surface (0-20 cm depth) decrease with depth to between 4-6% depending on the season at both sites (Fig. 11). Higher organic matter near the surface is consistent with the leaf litter on the surface and higher root density found near the surface from the floodplain soil pit. The floodplain site has about the same organic carbon percentage at each depth interval from fall to spring. The terrace site shows a slight variation in organic carbon percentage with the spring cores containing more organic carbon between the depth intervals of 50-100 cm.

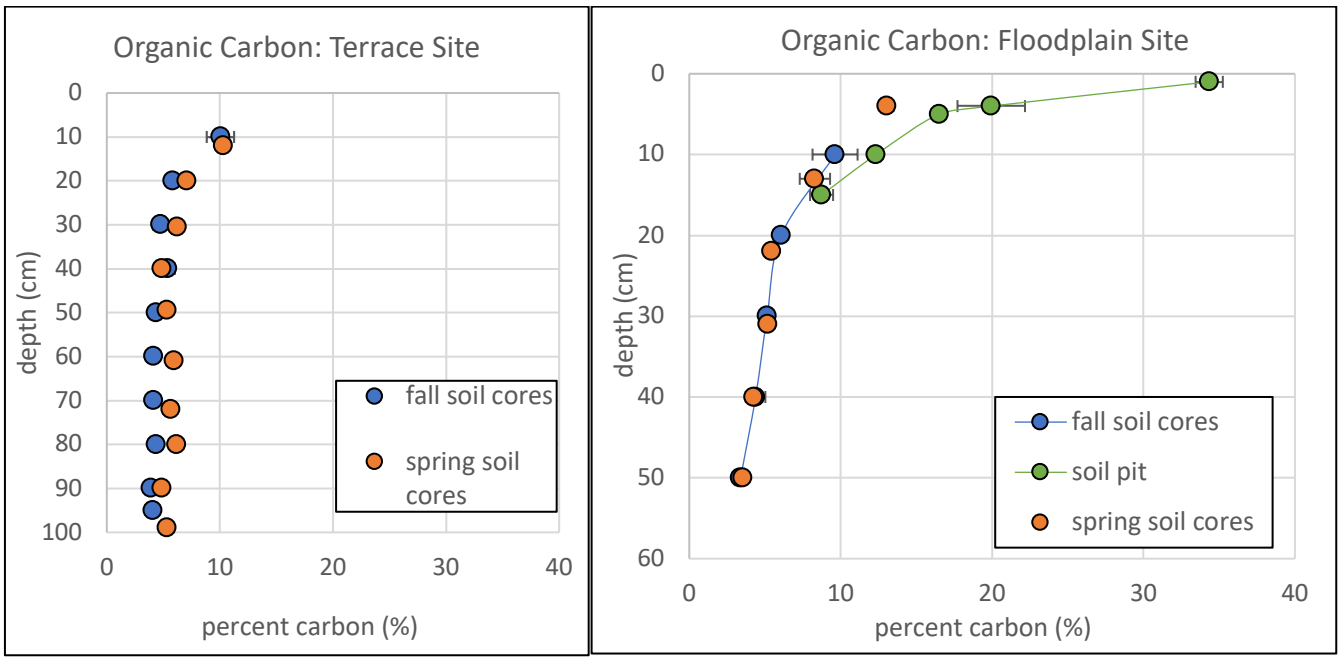

Fig. 11: The organic carbon percentage with depth for the terrace (left) and floodplain site (right) from the fall and spring soil cores. The organic carbon percentage from fall soil cores are the averages of multiple samples from the same depth. The error bars are standard deviation.

Grain Size

Grain size was determined by sieve analysis for samples obtained at interval in core samples. Fig. 12 shows these data from the terrace and floodplain site. The size of particles in each sample varies ranges from clay to coarse sand size particles, without systematic variation with depth. The largest particles on the terrace site are smaller than those on the floodplain site. Table 2 contains the error from the sieve grain size analysis, D_{50}, D_{90}, and the calculated capillary fringe rise for the terrace and floodplain site. D_{50} refers to median grain size, which represents the diameter corresponding to 50% finer in the particle-size distribution. D_{90} refers to the 90th percentile grain sizes, where ninety percent of distribution has a smaller particle size and ten percent has a larger particle size. The capillary fringe rises are calculated using the D_{50} and D_{90} found for each depth. The capillary fringe rise is calculated from both D_{50} and D_{90} indicts that the capillary fringe could go all the way to the surface. This doesn't match the field measurements, which indicates macroporosity is important factor in capillary fringe height. D_{90} has a lower calculated capillary fringe rise than D_{50}, which is constant with height of the capillary fringe above the water table is inversely related to pore size.

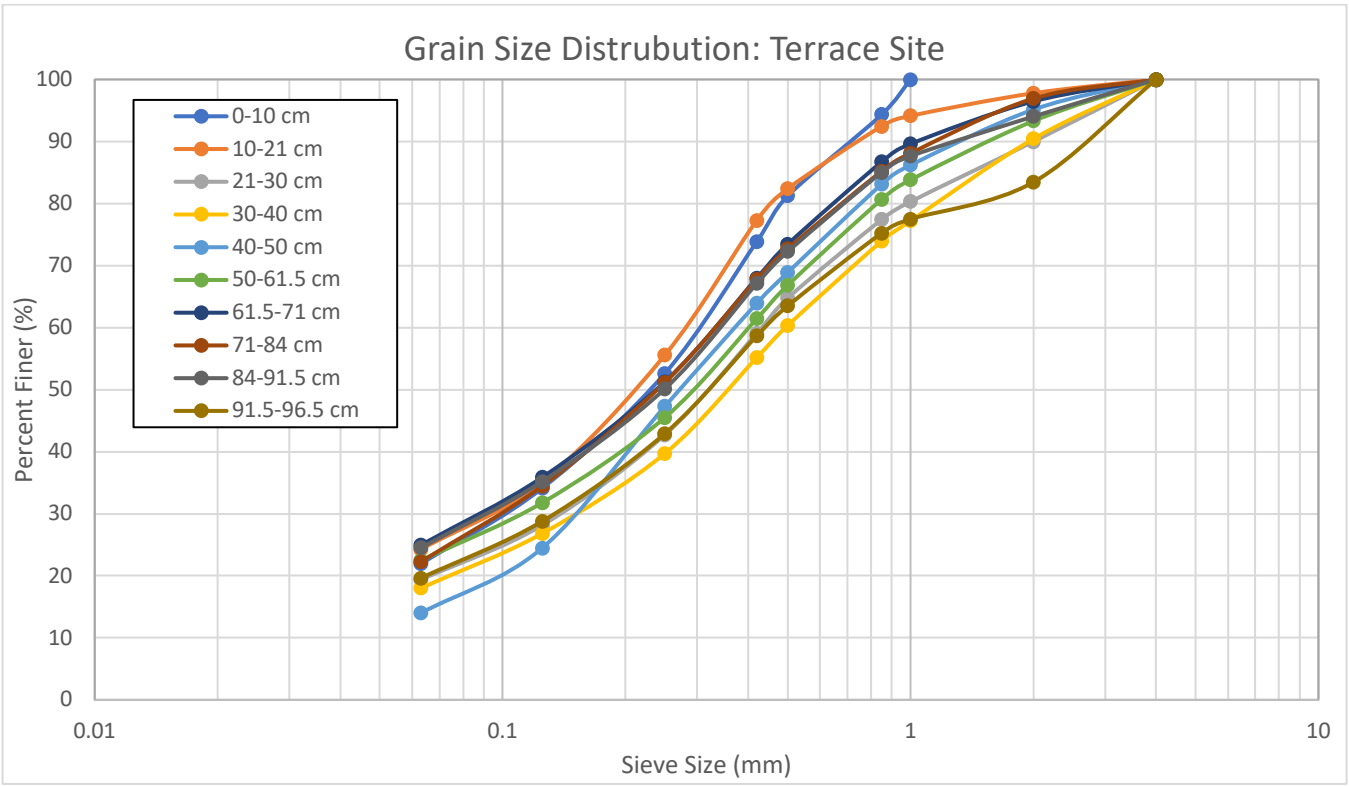

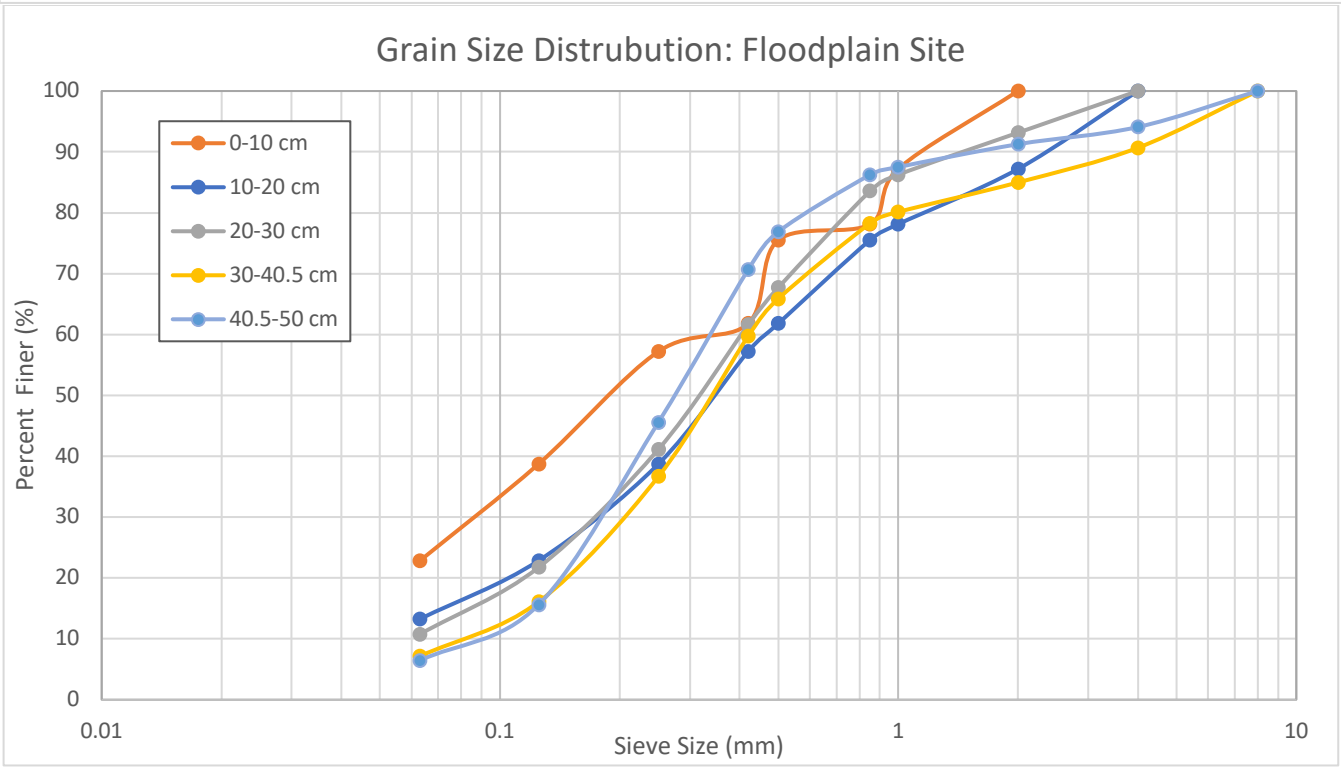

Fig. 12: Particle size distribution curves for each depth using sieve analysis for the terrace (top) and floodplain site (bottom).

Floodplain Site

Depth (cm)	Sieve Analysis Error (%)	D_{50} (mm)	Capillary Fringe Rise for D_{50} (m)	D_{90} (mm)	Capillary Fringe Rise for D_{90} (m)
0-10	2.27	0.19	156.38	1.2	24.76
10-20	0.79	0.27	110.05	2.5	11.89
20-30	0.18	0.32	92.85	1.5	19.81
30-40.5	0.23	0.34	87.39	3.9	7.62
40.5-50	0.80	0.35	84.89	1.6	18.57
Mean		0.29	106.31	2.14	16.53
Standard Deviation		0.07	29.66	1.10	6.78

Terrace Site

Depth (cm)	Sieve Analysis Error (%)	D_{50} (mm)	Capillary Fringe Rise for D_{90} (m)	D_{90} (mm)	Capillary Fringe Rise for D_{90} (m)
0-10	4.39	0.24	123.80	0.71	41.85
10-21	0.66	0.22	135.06	0.73	40.70
21-30	0.61	0.33	90.04	2	14.86
30-40	0.69	0.36	82.54	2	14.86
40-50	0.85	0.27	110.05	1.5	19.81
50-61.5	0.52	0.29	102.46	1.7	17.48
61.5-71	0.85	0.25	118.85	1	29.71
71-84	0.81	0.25	118.85	1.2	24.76
84-91.5	0.52	0.25	118.85	1.5	19.81
91.5-96.5	0.96	0.33	90.04	2.7	11.00
Mean		0.28	109.05	1.50	23.48
Standard Deviation		0.05	17.17	0.63	10.76

Table 2: Tables containing the error from the sieve grain size analysis, D_{50}, D_{90} and the calculated capillary fringe rise for the terrace and floodplain site. The capillary fringe rise is calculated using the median grain size (D_{50}) and D_{90}found for each depth.

Soil Infiltration Rate

During the fall of 2019, infiltration measurements were made at the floodplain site during dry soil conditions. Five sites were measured on the floodplain using falling head, single-ring infiltrometers with both 9.5 and 15.5 cm diameters. The rate of infiltration is determined from the slope of the liner best-fit line, which was convert from cm/s to cm/hr. These sites show a wide range of infiltration rates from 17 to 98 cm/hr (Fig. 13). The range of infiltration rates reflects both matrix and macropore infiltration at the floodplain site during dry conditions, which is consistent with the surface soils having high porosity and low bulk density. The 10/25/2019 measurement was taken after some precipitation, but the soil was still dry on the surface. The rate of infiltration on 10/25/2019 decreased due to the soil having more moisture than several weeks before.

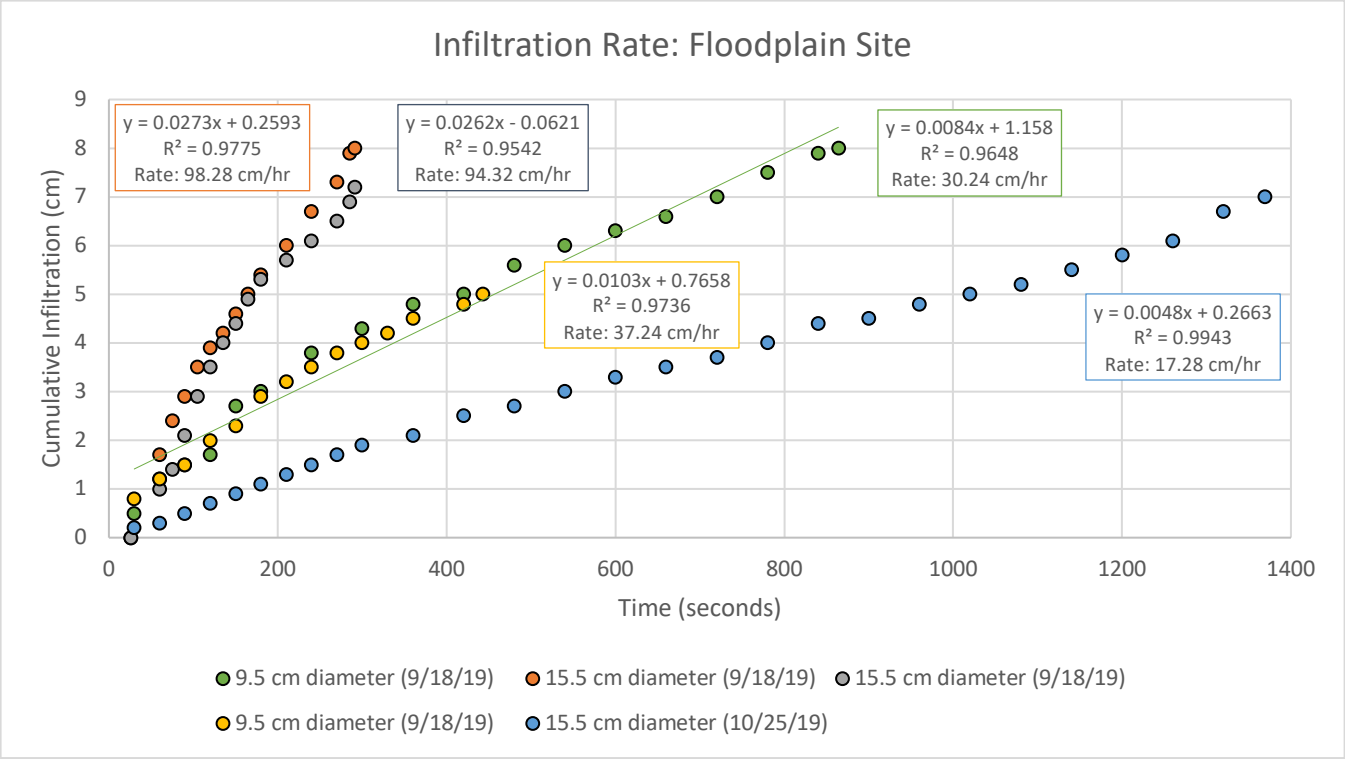

Fig. 13: Infiltration rates during the fall at the floodplain site. High infiltration rates are indictors of macroporosity and drier soil conditions.

Hydrological Measurements:

The hydrological data were obtained from groundwater wells at the study site and long-term hydrological measurements. Precipitation data were obtained Weather Underground station KMDHYATT15, which is recorded from a nearby rain gauge monitored by a citizen scientist. Long-term temperature and precipitation date were obtained from PRISM Climate Group, which uses long-term data from the National Climatic Data Center (PRISM 2020).

Precipitation and Groundwater Monitoring Data

The annual groundwater data from the terrace, floodplain, and hole wells are shown in Fig. 14. The groundwater well data was collected with Haley Talbot-Wendlandt, due to the size of the database, she processed the HOBO data and created the time series and groundwater probability figures. The groundwater well data show the water table is much lower during the summer months which corresponds to the increased ET and temperatures. The minimum groundwater table was between July to October for all sites. The water table begins to rise during the fall as evapotranspiration rates drop and it is at its highest during the winter. Also, the well data shows the capillary fringe response, which is the rapid response to precipitation events and recovering to its original depth during warm seasons when water is removed by roots. During the summer the recovery is rapid, and during the winter a slower smoother recovery is seen. Fig. 15 represents the terrace site groundwater probability curve, which provides the percent of the time the groundwater level will be at or above the indicated value. This groundwater probability graph was constructed for 4-time intervals: winter, spring, summer, and

fall. During the winter months when ET is low, the water table is near the surface. During the summer the water table retains similar values as it drops to a minimum. This suggests the water table has dropped below the rooting depth of the vegetation.

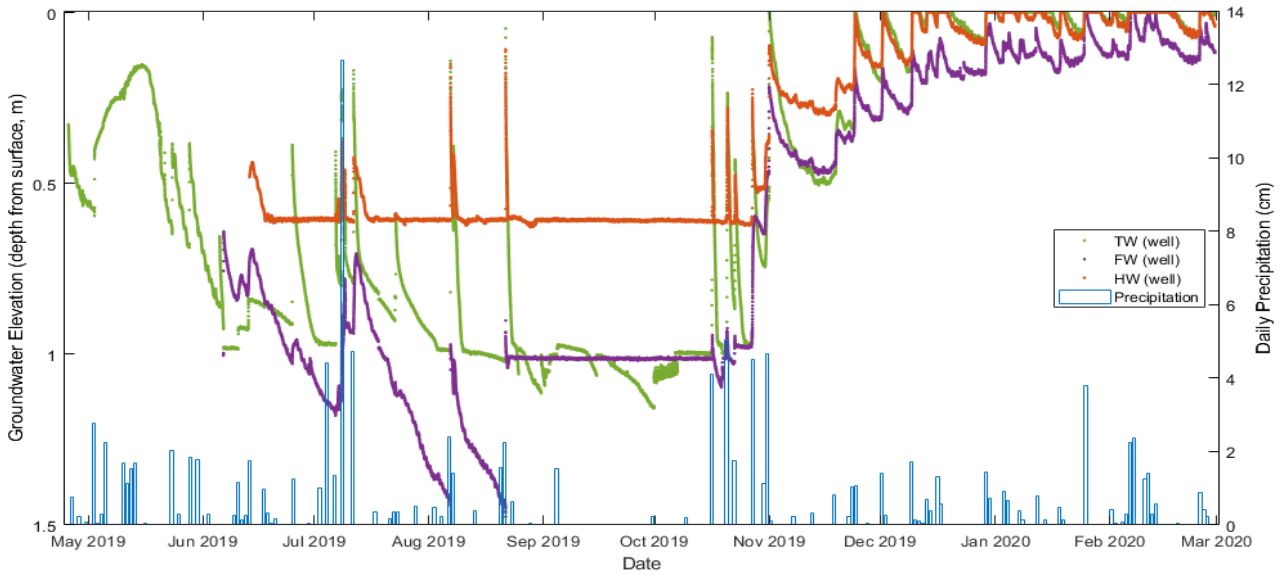

Fig. 14: Groundwater depth data recorded from all three wells on the Little Paint Branch floodplain. Precipitation data is from Weather Underground station KMDHYATT15. ("TW' Terrace Well, "FW" Floodplain Well, and "HW" Hole Well). (Weather Underground) (Credit: Haley Talbot-Wendlandt)

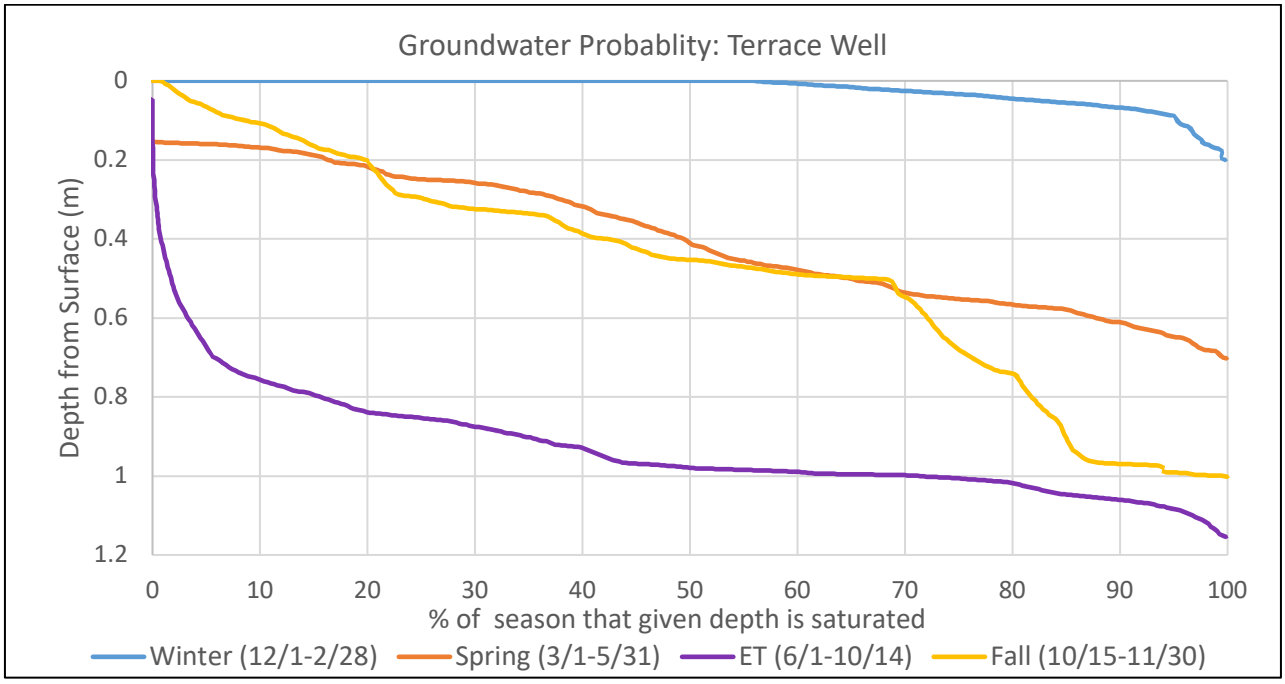

Fig. 15: Groundwater probability curve using groundwater well data from the Terrace site. The groundwater probability curve provides a percentage for each season that a specific depth will be saturated. ET represents the summer months. For example: the groundwater level is higher than 1 meter 60% of the time during the summer. (Credit: Haley Talbot-Wendlandt)

Precipitation and Temperature Data

Daily precipitation and temperature data were obtained from PRISM Climate Group for the period between 2009 to 2018 at the Little Paint Branch floodplain. I calculated the average of the maximum and minimum temperatures between this period (Fig.16) The temperature represent Maryland has seasonal variations in temperature. Fig 17 represents the average precipitation from this time frame, which shows a consistent rain fall throughout the year. This lack of seasonality in precipitation indicates that ET generates the seasonality in the water balance.

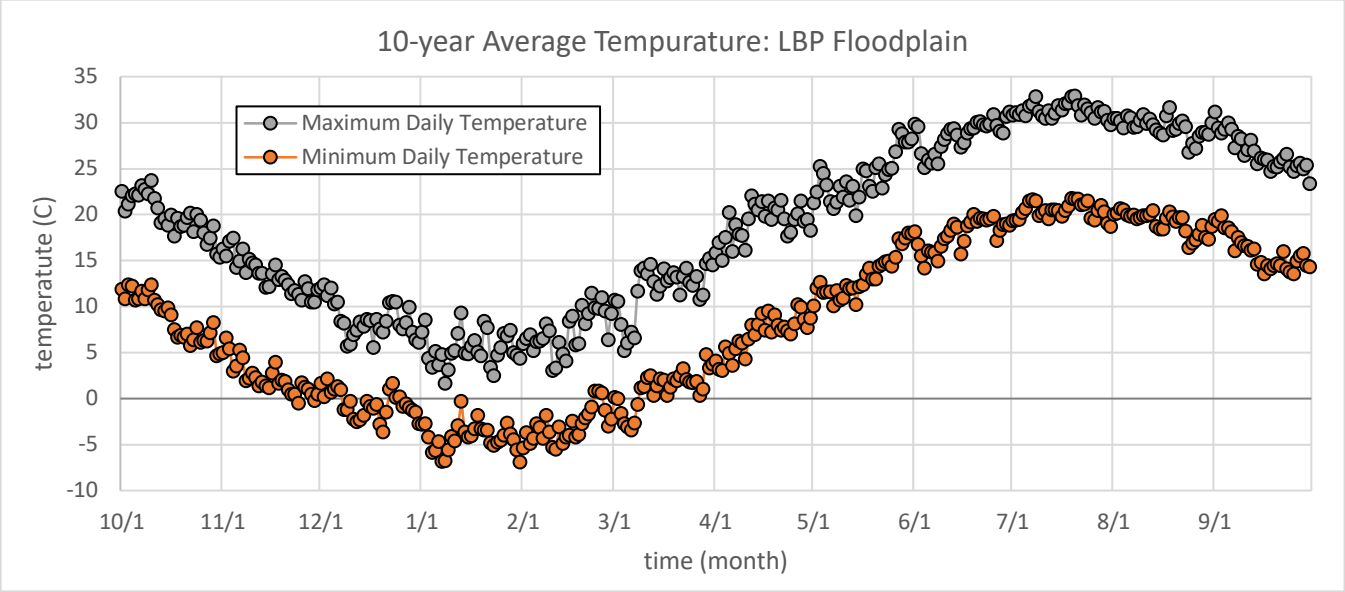

Fig. 16: The average maximum and minimum temperature between 2009 to 2018. (Calculated from data obtained PRISM Climate Group)

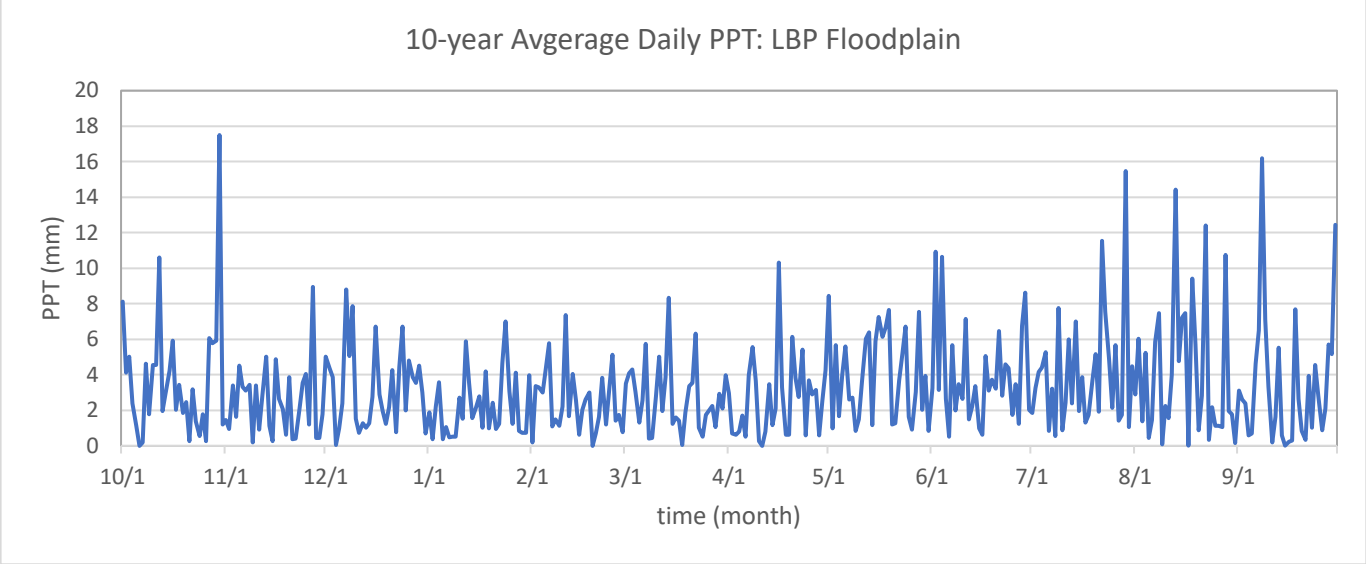

Fig. 17: Average daily precipitation between 2009 to 2018. (Calculated from data obtained from the PRISM Climate Group)

Results of Evapotranspiration Calculations

The daily ET was calculated from Hargreaves-Samani Equation using the maximum and minimum temperature data obtained from PRISM climate group (Ravazzani et al. 2012). Fig. 18 displays a clear oscillating pattern of ET, with high ET during the warm summer months and lower to near zero ET during the winter months. Fig. 18 displays the calculated 10-year average of daily ET for the LBP floodplain. Fig. 19 displays the change in groundwater storage for LPB floodplain using the calculated average precipitation minus calculated average ET. These data indicate that ground water storage is a positive term in the fall, which indicates groundwater recharge. Groundwater storage is a positive term until Mid-March, when the increase in ET begins to remove groundwater from storage. This storage term is negative throughout the spring and summer, reaching a maximum in late summer.

The change in groundwater storage can be converted to a change in groundwater level if the specific yield is known for various depth intervals in the soil (Fig. 20). The change in water level is calculated by ΔGroundwater Storage/ Specific Yield. In this study, I used a value of 0.05 for specific yield. This value was determined in a field study on similar soil by Winston (1994), who also studied evapotranspiration on forested floodplains in Maryland. These calculations suggest a range in water level of 0.5 meter. This is similar to the observed range at some of the field sites, but most showed a higher range of water level change. These differences could be due to variations in rooting depth, the position of the capillary fringe, groundwater drainage, and variations in specific yield in the soil profile. Fig. 21 displays the cumulative change in groundwater storage for LPB floodplain. The groundwater table is at its maximum in Mid-March then it begins to decline. This suggest in Mid-March the groundwater table is near the surface and the water table minimum excepted from these calculations is 0.5 m.

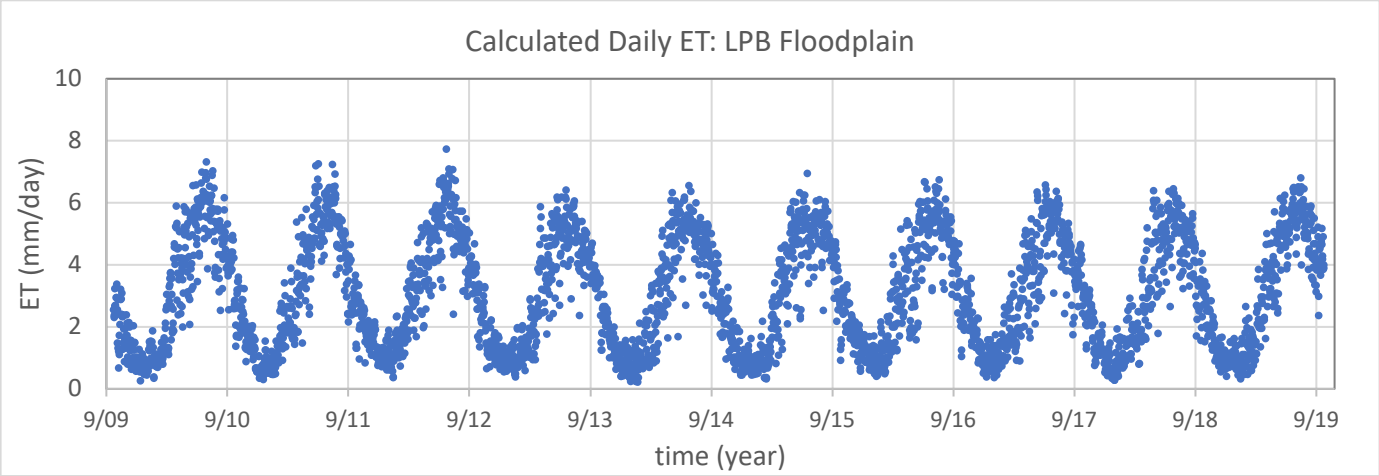

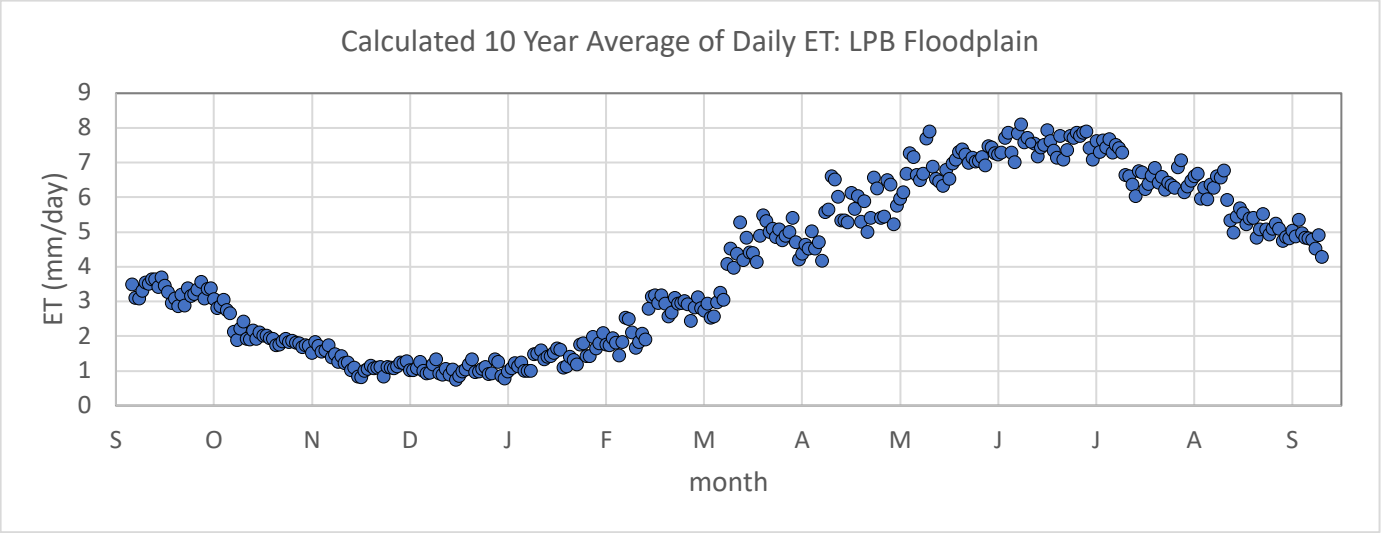

Fig. 18: (top) Average daily ET calculated using PRISM Climate data and the Hargreaves-Samani Equation for the water year for the interval 2009 to 2018. (bottom) A 10-year average of daily ET for Little Paint Branch Floodplain between 2009 to 2018. (PRISM Climate Group)

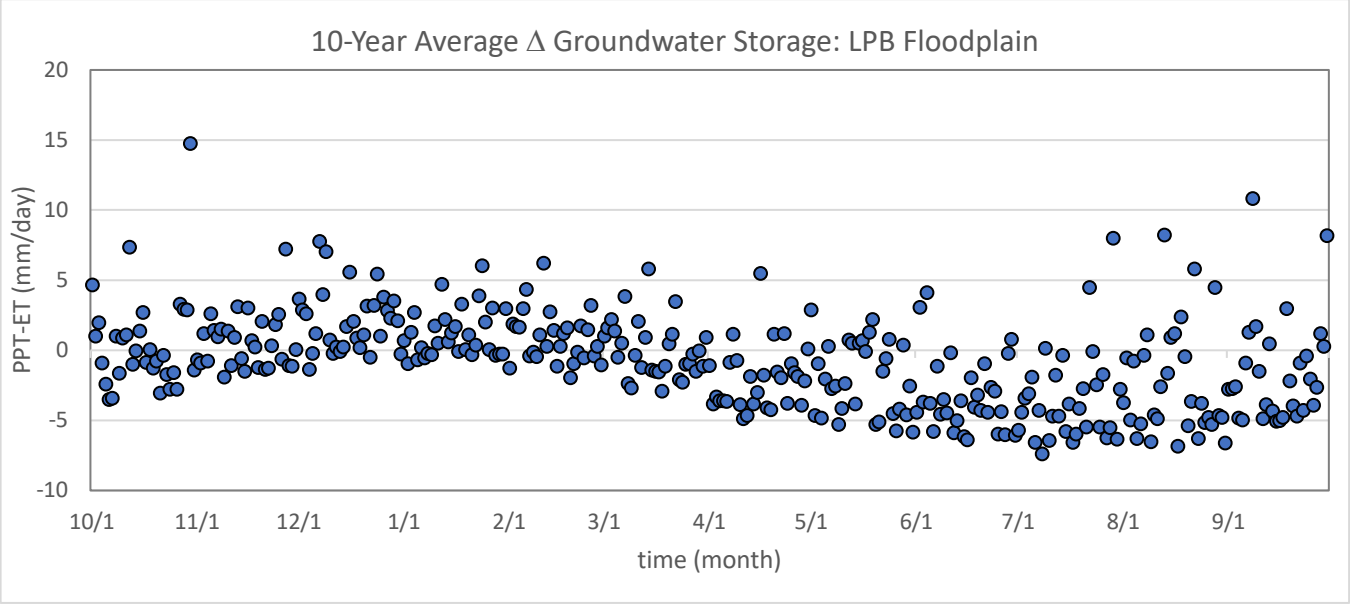

Fig. 19: Change in groundwater storage for LPB floodplain using the average daily ET and average daily PPT data calculated for Fig.20. (Calculated using data obtained for PRISM Climate Group)

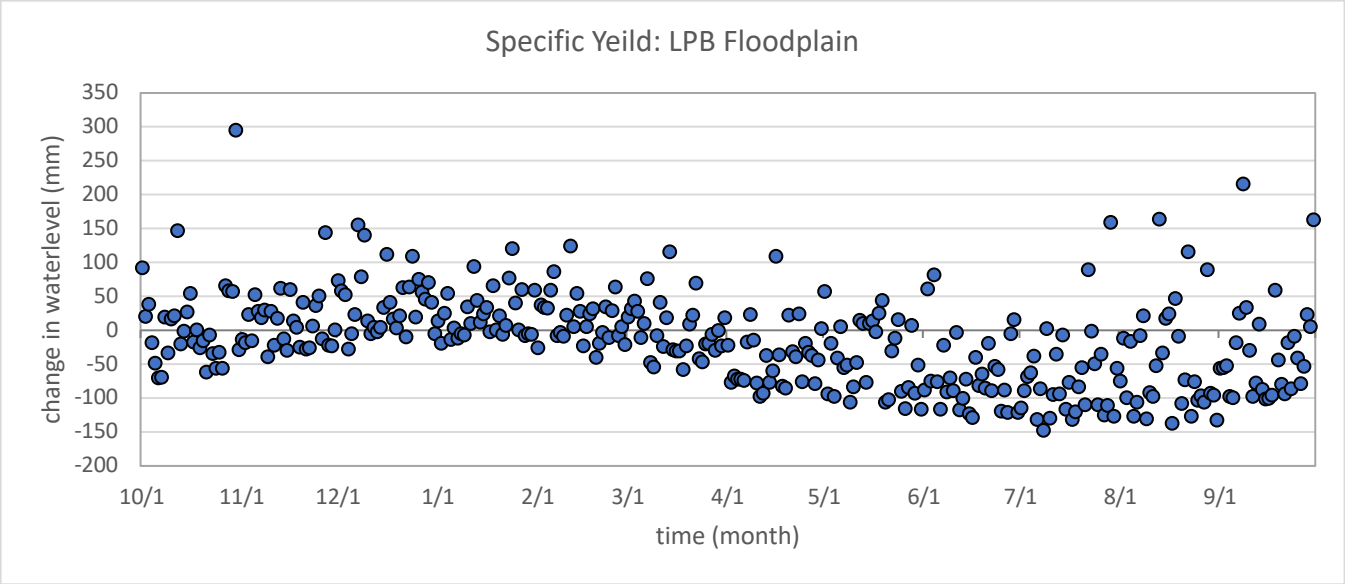

Fig. 20: The specific yield for LPB floodplain. (PRISM Climate Group)

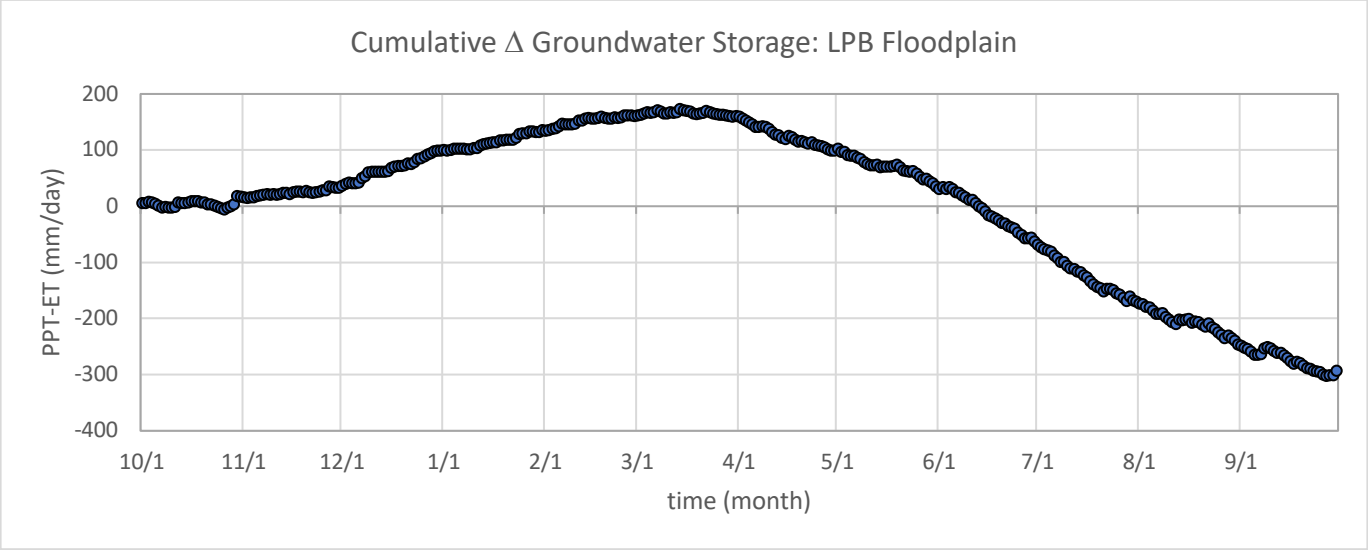

Fig. 21: Cumulative change in groundwater storage for LPB floodplain. (PRISM Climate Group)

Conclusion

Groundwater well data displays the water table declining during the summer months and recovering during the fall/winter months. An oscillating pattern is observed with ET and temperatures highest during the summer and lowest in the winter, which translates to the groundwater recharging during the winter and depleting during the summer. Mid-March the water table for LPB floodplain will be near the surface and at it maximum. This supports the hypothesis that groundwater minima are driven by evapotranspiration in excess of precipitation in Maryland, which removes groundwater storage creating groundwater minima in early autumn. Further research could include calculating daily ET from the groundwater well data and comparing it to PRISM data for the same sites.

The organic carbon was highest at the surface then decease with depth, which is consistent with leaf matter and roots in the near surface soils. Initial examination of the roots indicates high density of roots in the upper 20-30 cm of the floodplain soils. The grain size distributions are relatively similar for the different horizons in the soil and do not show systematic changes with depth. The bulk density increases with depth intervals at both sites, reaching values consistent with mineral soils with these grain sizes at depth (Dunne and Leopold, 1978). This suggests that the surface soil horizons have more or larger macropores, which is also indicated by the higher values of porosity in the surface soils. These variations in organic matter, bulk density, and porosity with depth without significant variations in grain size supports the hypothesis that soil characteristics exhibit vertical changes with depth and that these changes are due to biota (roots, leaf litter, worms, etc.), not grain size variations. Farther research is needed to understand the effects of the biota through excavation of roots interval depth at each site and calculating the root density at each depth.

The height of the potential capillary fringe calculated from the median and 90th percentile grain sizes are both significantly higher than observed capillary fringe responses. These data suggest that without macropores or removal by roots, the capillary fringe would be at the surface, creating wet conditions, which is observed in the winter period in absence of forest transpiration. Capillary fringe responses are larger in the deeper portions of the soil. This suggests that matrix pore size, which is assumed to be the same as grain size, may not be representative of macropore sizes that influence the rise of the capillary fringe. Bulk density and porosity data suggest that macropores are common especially in the upper portions of the soil at both locations.

The importance of this research is groundwater table depths, vegetation type, and their rooting depth are coupled and tied to the climate. The changing climate would affect the groundwater depth, which would cause changes in vegetation and growing season length. Also, groundwater probability distribution would provide an approach to evaluate the groundwater levels seasonally and suggest main rooting depths, and not just an average.

Acknowledgments

I would especially thank my advisor, Dr. Karen Prestegaard, for all of her guidance and assistance throughout my senior thesis and access to her hydrology lab. Also, special thanks to graduate student Haley Talbot-Wendlandt for her help with the groundwater well data and graphs.

References

Al-Shammary A A G, Kouzani A Z, Kaynak A, Khoo S Y, Norton M, Gates W. 2018. Soil Bulk Density Estimation Methods: A Review, *Pedosphere*, v. 28, n. 4, p. 581–596, doi: 10.1016/S1002-0160(18)60034-7.

Bear, J., 1972, Dynamics of fluids in porous media: New York, N.Y, Dover Publications.

Beven, K., and Germann, P., 1982, Macropores and Water Flow in Soils: *Water Resources Research*, v. 18, n. 5, p. 1311–1325, doi:10.1029/wr018i005p01311.

Cloke, H.L., Anderson, M.G., Mcdonnell, J.J., and Renaud, J.-P., 2006, Using numerical modelling to evaluate the capillary fringe groundwater ridging hypothesis of streamflow generation: *Journal of Hydrology*, v. 316, p. 141–162, doi: 10.1016/j.jhydrol.2005.04.017.

Dunne, T. and Leopold, L.B. (1978) Water in Environmental Planning. WH Freeman and Co., New York.

Fan, Y., Miguez-Macho, G., Jobbágy, E.G., Jackson, R.B., and Otero-Casal, C., 2017, Hydrologic regulation of plant rooting depth: *Proceedings of the National Academy of Sciences*, v. 114, p. 10572–10577, doi: 10.1073/pnas.1712381114.

Gribovszki, Z., Kalicz, P., Szilágyi, J., and Kucsara, M., 2008, Riparian zone evapotranspiration estimation from diurnal groundwater level fluctuations: *Journal of Hydrology*, v. 349, p. 6–17, doi: 10.1016/j.jhydrol.2007.10.049.

Hargreaves, G. H., 1994, Defining and Using Reference Evapotranspiration: *Journal of Irrigation and Drainage Engineering*, v. 120, n. 6, p. 1132–1139., doi:10.1061/(asce)0733-9437(1994)120:6(1132).

Heath, Ralph C., 1983, Basic ground-water hydrology: U.S. Geological Survey Water-Supply Paper 2220, 86 p.

Lehmann, J., and Kleber, M., 2015, The contentious nature of soil organic matter: *Nature*, v. 528, p. 60–68, doi: 10.1038/nature16069.

Munsell soil color charts, 1975, Baltimore, MD, Munsell Color.

Nimmo, J.R., Schmidt, K.M., Perkins, K.S., and Stock, J.D., 2009, Rapid Measurement of Field-Saturated Hydraulic Conductivity for Areal Characterization: *Vadose Zone Journal*, v. 8, p. 142–149, doi: 10.2136/vzj2007.0159.

PRISM Climate Group, Oregon State University, http://prism.oregonstate.edu, created 6 Nov 2019.

Ravazzani, G., Corbari, C., Morella, S., Gianoli, P., and Mancini, M., 2012, Modified Hargreaves-Samani Equation for the Assessment of Reference Evapotranspiration in Alpine River Basins: *Journal of Irrigation and Drainage Engineering*, v. 138, p. 592–599, doi: 10.1061/(asce)ir.1943-4774.0000453.

USGS, Groundwater is the area underground where openings are full of water, https://www.usgs.gov/media/images/groundwater-area-underground-where-openings-are-full-water (accessed November 2019).

Weather Underground, IBM, The Weather Channel, 2019, Station Cool Spring Terrace - KMDHYATT15 Weather Underground, precipitation table data, https://www.wunderground.com/dashboard/pws/KMDHYATT15 (accessed October 2019).

Winston, R.B., 1994, Seasonal variations in the water balance of a riparian wetland, Maryland Coastal Plain, Univ. of Maryland Ph.D. Disseration, 294 pp.

Zhang, J., Lei, T., Qu, L., Chen, P., Gao, X., Chen, C., Yuan, L., Zhang, M., and Su, G., 2017, Method to measure soil matrix infiltration in forest soil: *Journal of Hydrology*, v. 552, p. 241–248, doi: 10.1016/j.jhydrol.2017.06.032.

Zhang, L., Walker, G. R. and Dawes, W. R., 2002, Water Balance Modelling: Concepts and Applications: *Regional Water and Soil Assessment for Managing Sustainable Agriculture in China and Australia*, no. 84, p. 31-47.

Honor code: I pledge on my honor that I have not given or received any unauthorized assistance on this assignment.
Samantha Volz

Appendix

GPS Latitude and Longitude for Each Site on the LPB Floodplain

Site observations	Elevation (m ASL, approximation)	Location in LPB system	GPS latitude	GPS longitude
Terrace	24.45	Terrace	38.99815	-76.93987
Floodplain	20.702	Floodplain	38.99722	-76.93801
Holes	20.647	Floodplain	38.99712	-76.93750

Table 3: Elevation, GPS latitude, and GPS longitude for each study site in the LPB system. (Credit: Haley Talbot-Wendlandt)

Root Pictures from the Floodplain Site

Fig. 22: (Left and center) Roots from the organic horizon at the floodplain. (Right) The leaf litter removed from the 1 x 1 m soil pit at the floodplain site.

Munsell Soil-Color Chart

Table 4 is the soil color from the terrace and floodplain sites soil cores using the Munsell Soil-Color Chart.

Terrace Soil (10/16/19)

depth (cm)	hue (YR)	value	color
0-10	10	5/2	grayish brown
10-20	10	5/2	grayish brown
20-30	10	5/4	yellowish brown
30-41	10	5/4	yellowish brown
41-50	2.5	5/4	light olive brown
50-61.5	10	5/6	yellowish brown

61.5-70	2.5	5/6	light olive brown
70-79	10	5/6	yellowish brown

Terrace Soil (10/18/19)

depth (cm)	hue (YR)	value	color
0-10	10	4/2	dark grayish brown
10-21	2.5	4/2	dark grayish brown
21-30	2.5	4/4	olive brown
30-40	2.5	4/4	olive brown
40-50	2.5	5/6	light olive brown
50-61.5	2.5	5/6	light olive brown
61.5-71	10	5/8	yellowish brown
71-84	10	5/6	yellowish brown
84-91.5	2.5	5/4	light olive brown
91.5-96.5	2.5	5/4	light olive brown

Floodplain Soil (10/16/19)

depth (cm)	hue (YR)	value	color
0-11	2.5	4/4	olive brown
11-20	2.5	4/4	olive brown
20-30	10	5/4	yellowish brown
30-40	10	5/6	yellowish brown

Floodplain Soil (10/18/19)

depth (cm)	hue (YR)	value	color
0-10	10	3/2	very dark grayish brown
10-20	10	3/4	dark yellowish brown
20-30	10	4/6	dark yellowish brown
30-40.5	7.5	4/6	strong brown
40.5-50	10	4/6	dark yellowish brown

Table 4: The Munsell soil-color for each depth interval for the terrace and floodplain sites on 10/16/19 and 10/18/19.

Bulk Density and Porosity Data

Floodplain Site (10/16/19)

Depth (cm)	Dry Bulk Density (g/cm^3)	Field Bulk Density (g/cm^3)	Porosity (%)
0-11	0.78	0.84	70.45
11-20'	1.05	1.13	60.32
20-30	1.31	1.42	50.45
30-40	1.13	1.23	57.38

Terrace Site (10/16/19)

Depth (cm)	Dry Bulk Density (g/cm^3)	Field Bulk Density (g/cm^3)	Porosity (%)
0-10	0.61	0.69	76.92
10-20'	1.09	1.22	58.73
20-30	1.05	1.19	60.25
30-41	1.19	1.35	55.18
41-50	1.09	1.25	58.85
50-61.5	1.12	1.28	57.92
61.5-70	1.04	1.19	60.69
70-79	0.85	0.97	67.90

Floodplain Site (10/18/19)

Depth (cm)	Dry Bulk Density (g/cm^3)	Field Bulk Density (g/cm^3)	Porosity (%)
0-10	0.69	0.90	73.85
10-20'	1.05	1.27	60.26
20-30	1.05	1.24	60.40
30-40.5	1.21	1.35	54.49
40.5-50	1.27	1.38	52.25

Terrace Site (10/18/19)

Depth (cm)	Dry Bulk Density (g/cm^3)	Field Bulk Density (g/cm^3)	Porosity (%)
0-10	0.58	0.70	77.97
10-21'	0.86	1.00	67.60
21-30	0.92	1.07	65.17
30-40	1.12	1.29	57.84
40-50	1.10	1.28	58.48
50-61.5	2.31	1.17	12.71
61.5-71	1.09	1.29	58.74
71-84	1.21	1.42	54.48
84-91.5	1.34	1.54	49.47
91.5-96.5	1.43	1.63	45.93

Floodplain Site (3/18/20)

Depth (cm)	Dry Bulk Density (g/cm^3)	Field Bulk Density (g/cm^3)	Porosity (%)
0-13	0.59	0.77	77.71
13-22	0.62	0.76	76.79
22-31	0.73	0.86	72.39
31-40	0.83	0.97	68.55
40-50	1.54	1.80	41.99

Terrace Site (3/18/20)

Depth (cm)	Dry Bulk Density (g/cm^3)	Field Bulk Density (g/cm^3)	Porosity (%)
0-12	0.50	0.71	81.00
12-20'	0.81	1.09	69.45
20-30.5	1.01	1.27	61.85
30.5-40	0.93	1.22	64.80
40-49.5	0.94	1.29	64.50
49.5-61	1.29	1.72	51.48
61-72	0.93	1.27	64.91
72-80	1.12	1.54	57.63
80-90	1.25	1.63	52.69
90-99	1.29	1.61	51.22

Table 5: Dry bulk density, field bulk density, and porosity for the terrace and floodplain sites from all the soil cores.

Organic Carbon

Fig. 23: Soil before (left) and after (right) it was put in the kiln for the organic carbon analysis. Note the change in color.

Terrace: Fall Soil Core

Depth (cm)	Average Organic Carbon (%)	Standard Deviation
0-10	10.05	1.21
10-20	5.82	0.54
20-30	4.73	0.63
30-40	5.39	0.62
40-50	4.38	0.33
50-60	4.14	0.28
60-70	4.15	0.30
70-80	4.37	0.30
80-90	3.91	0.19
90-95	4.09	0.49

Terrace: Spring Soil Core

Depth (cm)	Average Organic Carbon (%)	Standard Deviation
0-12	10.31	0.35
12-20	7.10	0.16
30.5-40	4.86	0.35

Floodplain: Fall Soil Core

Depth (cm)	Average Organic Carbon (%)	Standard Deviation
0-10	9.63	1.49
10-20	6.07	0.34
20-30	5.14	0.39
30-40	4.38	0.64
40-50	3.39	0.28

Floodplain: Soil Pit

Depth (cm)	Average Organic Carbon (%)	Standard Deviation
0-1	34.34	0.90
1-4	19.94	2.23
4-5	16.51	0.01
5-10	12.34	0.23
10-15	8.74	0.76

Floodplain: Spring Soil Core

Depth (cm)	Average Organic Carbon (%)	Standard Deviation
0-4	13.05	0.42
0-13	8.30	1.00

Table 5: The fall soil cores combine both samples obtained on 10/16/2019 and 10/18/2019 for the average organic carbon with depth and standard deviation for the terrace and floodplain site. The floodplain soil pit measurements were taken between December 2019 to January 2020 in intervals. The spring soil cores were taken on 3/18/2020. Due to lack of access to the hydrology lab only some samples were able to have an average organic carbon and standard deviation.

Sieve Grain Size Raw Data

Floodplain Site

Depth (cm)	0-10	10-20	20-30	30-40.5	40.5-50
Sieve Size (mm)	**soil weight (g)**	**soil weight (g)**	**soil weight (g)**	**soil weight (g)**	**soil weight (g)**
4	0	0	0	15.9	8.8
2	0	22.6	11.2	9.7	4.2
1	18.4	16	11.3	8.3	5.6
0.85	3	4.6	4.4	3.2	1.9
0.5	12.5	24.2	25.9	21.1	13.9
0.42	4.2	8.1	10	10.5	9.3
0.25	13.3	32.6	33.4	39.3	37.3
0.125	13.4	28	31.7	35.1	44.6
0.063	10.5	16.9	17.9	15.2	13.6
pan	15.3	23.4	17.6	12.2	9.6
total (g)	90.6	176.4	163.4	170.5	148.8
original soil weight (g)	92.7	177.8	163.7	170.9	150

Terrace Site

Depth (cm)	0-10	10-21	21-30	30-40	40-50	50-61.5	61.5-71	71-84	84-91.5	91.5-96.5
Sieve Size (mm)	**soil weight (g)**	**soil weight (g)**	**soil weight (g)**	**soil weight (g)**	**soil weight (g)**	**soil weight (g)**	**soil weight (g)**	**soil weight (g)**	**soil weight (g)**	**soil weight (g)**
2	0	2	14.7	12.4	5.7	7.7	3.3	3	5.7	10.3
1	0	3.3	14.2	17.1	10.5	10.9	6.4	8.6	6.1	3.7
0.85	4.3	1.5	4.2	4.2	3.6	3.6	2.7	2.8	2.5	1.4
0.5	10	9.1	18.6	17.6	16.7	15.9	12.4	12.2	12.2	7.3
0.42	5.6	4.6	8.3	6.7	5.8	6.2	5.1	4.8	4.9	3
0.25	16.2	19.6	24	20	19.5	18.3	15.6	16.2	16.2	9.8
0.125	14.1	18.5	21.4	16.7	26.8	15.8	14.4	16.3	14.3	8.8
0.063	9.3	9.8	12.9	11.4	12.3	10.7	10.2	11.9	10.2	5.7
pan	16.7	21.9	28.4	23.3	16.4	25.8	23.3	21.7	23.4	12.2
total (g)	76.2	90.3	146.7	129.4	117.3	114.9	93.4	97.5	95.5	62.2
original soil weight (g)	79.7	90.9	147.6	130.3	118.3	115.5	94.2	98.3	96	62.8

Table 6: Sieve grain size analysis raw data for both the floodplain and terrace site.